# Martensitic and room-temperature magnetocaloric properties of Mn-rich Mn-Ni-Sn Heusler alloys: Experiment and theory

Jyoti Sharma,[1] A. A. Coelho,[2] K. G. Suresh,[3] and Aftab Alam[1,*]

[1]*Materials Modeling Laboratory, Department of Physics, Indian Institute of Technology Bombay, Mumbai 400076, India*
[2]*Instituto de Física 'Gleb Wataghin', Universidade Estadual de Campinas-UNICAMP, CP 6165, Campinas, Sao Paulo, 13, 083970, Brazil*
[3]*Magnetic Materials Laboratory, Department of Physics, Indian Institute of Technology Bombay, Mumbai 400076, India*

(Received 26 November 2023; revised 5 February 2024; accepted 7 February 2024; published 21 February 2024)

Here, we study the effect of external pressure on martensitic transition, magnetic, and magnetocaloric properties of Mn-rich $Mn_{50}Ni_{41-x}Sn_{9+x}$ ($x = 0$ and 2) Heusler alloys by using a combined experimental and first principles simulation. The $x = 0$ alloy exhibits martensitic transition around room temperature (RT), which increases appreciably under external pressure for both the alloys. External pressure and magnetic field show opposite effects on martensitic transition ($T_M$). The $x = 0$ alloy shows a maximum isothermal magnetic entropy change ($\Delta S_M$) of 6.5 J/kg K under ambient pressure at RT, which is comparatively larger than that reported in many other Heusler systems at RT. Interestingly, $\Delta S_M$ decreases with pressure for $x = 0$, while it shows an increasing trend for $x = 2$. A maximum refrigeration capacity of around 79 J/kg is observed for $x = 0$. Similar to the magnetic entropy change, the net magnetization for $x = 0$ and $x = 2$ show opposite trend under external pressure. This is explained by our *ab initio* simulation by closely inspecting the consequence of nonuniform strain along three crystallographic directions on the net magnetization. This actually arises due to considerable magnetocrystalline anisotropy in these alloys. The unconventional mechanism behind the influence of pressure on magnetic properties is also discussed in the light of varying bond lengths between different magnetic species, and hence on the antiferromagnetic/ferromagnetic exchange coupling strengths under pressure.

DOI: 10.1103/PhysRevB.109.064418

## I. INTRODUCTION

In the last few decades, environment friendly, low-energy consumption and cost-effective magnetic refrigeration technology based on magnetocaloric effect (MCE) has emerged as a potential alternative to the conventional gas-based refrigeration technology. Discovery of giant MCE at room temperature (RT) in $Gd_5(Si_2Ge_2)$ around the first-order phase transition has attracted a great deal of attention of research community, to search the new materials for RT magnetic refrigeration application [1]. MCE is defined as the heating or cooling of a matter, when it is exposed to the variations of magnetic field, and manifested in terms of isothermal magnetic entropy change ($\Delta S_M$) or the adiabatic temperature change ($\Delta T_{ad}$) [2]. Generally, large MCE has been found in materials, which exhibit first-order magnetostructural transition, owing to the large magnetization difference ($\Delta M$) between two phases [1,3]. Multifunctional Ni-Mn based Heusler alloys have emerged as a potential candidate along this line, as most of these alloys show the first-order magnetostructural transition (i.e., the martensitic transition) from high-temperature cubic austenite phase to low-temperature tetragonal/orthorhombic/monoclinic martensite phase [4–8]. Additionally, their various physical properties such as large MCE, shape memory effect, large exchange bias, magnetostriction, large magnetothermal conductivity, and giant magnetoresistance (MR), etc., render them truly multifunctional, and lead to various potential applications [4–8]. Most of their properties can be simply tuned by changing either the composition (chemical pressure) or external (i.e., hydrostatic) pressure. Magnetic properties of these Ni-Mn based alloys are mainly controlled by the magnetic moment of Mn atoms. The later, in turn, depends on the interatomic distance between Mn atoms and also on the nonmagnetic ligand atoms connecting two further neighboring Mn atoms. Therefore, any change in the Mn-Mn distance can lead to the modification in Mn-Mn antiferromagnetic (AFM)/ferromagnetic (FM) exchange interactions in these alloys, and consequently affects their physical properties.

In general, application of external pressure is found to play a crucial role to influence the magnetic and structural transitions owing to a strong influence on the interatomic distances, and consequently the AFM/FM exchange interactions in Ni-rich (Ni 50 at.%) Ni-Mn-$Z$ ($Z$ = Ga, In, Sb, Sn) alloys. For instance, it is reported to significantly affect physical properties such as magnetic, MCE, and MR etc. [8–11]. Apart from this, in $Ni_{48}Mn_{39}Sn_{13-x}Si_x$ alloys, martensitic transition temperature is found to increase with respect to pressure at the rate of 2.37 K/kbar and 0.7 K/kbar for $x = 1$ and 4 respectively [11]. More recently, Mn rich (Mn 50 at.%) Mn-Ni-$Z$ ($Z$ = Sn, Ga, In) Heusler alloys have attracted a greater deal of attention, as compared to the Ni-rich Heusler alloys, owing to the stronger AFM/FM exchange interactions as a result of excess Mn content, which leads to significant enhancement in various physical properties as mentioned above

*aftab@iitb.ac.in

 

[12–16]. However, only a few pressure dependent studies are available in literature on these Mn-rich (Mn 50 at.%) Heusler alloys. Therefore, it would be interesting to explore the effect of pressure on their physical properties, such as martensitic transition, magnetic, and MCE.

In the present paper, we have studied the effect of pressure on martensitic transition, magnetic, and magnetocaloric properties of Mn-rich $Mn_{50}Ni_{41-x}Sn_{9+x}$ ($x = 0$ and 2) alloys. We have observed the room-temperature MCE for $x = 0$ alloy, which is found to decrease with increasing pressure, but follows an opposite trend for $x = 2$ alloy. In order to further understand the microscopic origin of the effect of pressure on their magnetic and magnetocaloric properties, we have performed the pressure dependent first-principles density functional theory (DFT) calculations. Both the alloys have been found to show a unique ferrimagnetic (FiM) ground state, with two Mn atoms (on two different sublattices) oppositely aligned, partially compensating each other giving rise to net magnetization. Pressure is found to affect their magnetic properties significantly. The change in the bond lengths between different Mn atoms with varying pressure and its corresponding effects on magnetism explains the experimental findings fairly well. Other experimental results are also discussed and compared with simulated data.

## II. EXPERIMENTAL AND COMPUTATIONAL DETAILS

Polycrystalline samples of $Mn_{50}Ni_{41-x}Sn_{9+x}$ ($x = 0$ and 2) Heusler alloys were prepared by arc melting method under pure argon atmosphere. After melting, samples were annealed in an evacuated quartz tubes at 1073 K for 70 h and then quenched in liquid nitrogen, to get better homogeneity. Structural analysis is performed using the x-ray diffraction (XRD) pattern obtained at room temperature (RT) employing PANalytical Xpert PRO diffractometer. Magnetization measurements at various applied pressures were carried out using the superconducting quantum interference device (SQUID) magnetometer (quantum design) attached with a CuBe clamp type pressure cell with a maximum pressure limit of 12 kbar. DC magnetization vs temperature (M vs T) data in zero field cooling (ZFC) and field cooled cooling (FCC) modes, in different measuring fields (up to 70 kOe) were also recorded using the SQUID magnetometer. Throughout the present paper, ambient pressure (0.001 kbar) is denoted by $P = 0$.

First-principles calculations are performed using density functional theory as implemented in Vienna *Ab Initio* Simulation Package (VASP), within the projected augmented wave (PAW) formalism. We have adopted the generalized gradient approximation as proposed by Perdew Burke-Ernzerhof (PBE) to incorporate the exchange and correlation effects. An energy cut-off of 350 eV has been used in all the calculations. Total energy (force) is converged up to $10^{-6}$ eV/cell (0.01 eV/Å). Brillouin zone (BZ) integration of the conventional unit cell of stoichiometric $Mn_2NiSn$ alloy is performed using the Γ-centered 8×8×8 k mesh. Off-stoichiometric $Mn_{50}Ni_{41-x}Sn_{9+x}$ alloys are simulated using a 2×2×2 supercell of the conventional unit giving rise to the off-stoichiometric compositions close to experimental ones. For these calculations, 6×6×6 k mesh is used for the BZ integration.

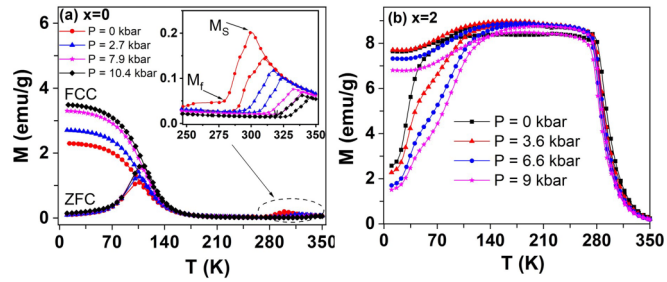


FIG. 1. For $Mn_{50}Ni_{41-x}Sn_{9+x}$ Heusler alloy, ZFC and FCC, magnetization (M) vs temperature (T) curves at different external pressure for (a) $x = 0$ and (b) $x = 2$ at 100 Oe field. Inset in (a) shows a zoomed-in view of M vs T curves near the inflection point.

## III. RESULTS AND DISCUSSIONS

### A. Experiment

The XRD data and the corresponding analysis for both the alloys ($x = 0$ and 2) is shown in the Supplemental Material (SM) [17]. The LeBail refinement using FullProf suite software confirms that the composition $x = 0$ possess a mixed phase involving a tetragonal (space group I4/mmm) and cubic (space group $Fm\bar{3}m$) structure at RT with the estimated lattice parameters a = b = 5.27 Å, c = 7.10 Å (c/a ratio = 1.35) for tetragonal phase, and a = b = c = 5.72 Å for the cubic phase respectively. This suggests that this alloy may possess the martensitic transition at/around RT. Increasing the composition to $x = 2$ transforms the system to a purely cubic structure (space group $Fm\bar{3}m$) at RT, with the estimated lattice parameters a = b = c = 6.01 Å, which indicates that it may show the martensitic transition below RT. It is generally known that most of the Ni-Mn based Heusler alloys exhibit the first-order martensitic transition from high-temperature cubic austenite (A) phase to low-temperature tetragonal/orthorhombic/monoclinic martensite (M) phase. In Mn-rich Mn-Ni-Sn alloys, the coupling between regular Mn atoms and Mn atoms occupying Ni and Sn sites are predominantly AFM type due to decrease in interatomic distances less than a critical value. This is also evident in our present case, e.g., for composition $x = 0$, the first- and second-nearest-neighbor distance between Mn atoms are 2.28 Å and 2.64 Å respectively. Therefore, these Mn atoms would couple antiferromagnetically. With the increase of x, i.e., for composition $x = 2$, the first- and second-nearest-neighbor distances between Mn atoms become 2.60 Å and 3.00 Å respectively, owing to the increase in lattice parameters. This is indicative of the increase in FM coupling with increasing x (Sn content) in the alloy. These experimental findings are in fair agreement with our theoretical results, shown later.

Figures 1(a) and 1(b) show the ZFC and FCC magnetization (M) vs T curves for the two alloys ($x = 0,2$) measured in 100 Oe field, under external pressures ranging from 0 to 10.4 kbar. From Fig. 1(a) for $x = 0$ alloy, it can be seen that at ambient pressure, on decreasing the temperature, the alloy undergoes a transition from austenite to martensite phase with a sharp jump in magnetization at 305 K (around RT). This sharp jump corresponds to the martensitic start temperature ($M_s$) and attains the minimum magnetization value at the

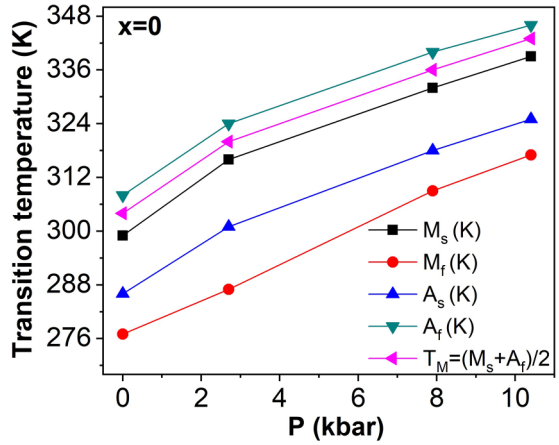


FIG. 2. For $Mn_{50}Ni_{41-x}Sn_{9+x}$ Heusler alloy, variations of characteristic martensitic transition temperatures [$M_s$, $M_f$, $A_s$, $A_f$ and $T_M = (M_s+M_f)/2$] as a function of pressure for $x = 0$ alloy.

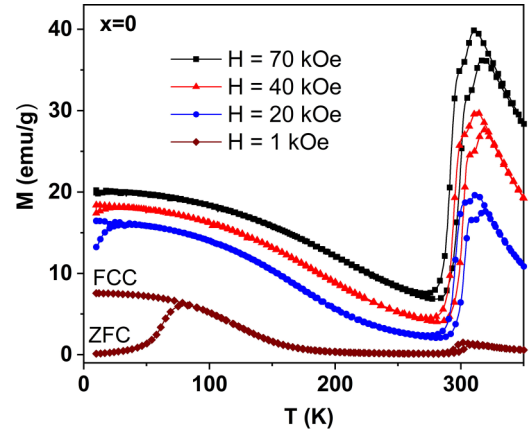


FIG. 3. For $Mn_{50}Ni_{41-x}Sn_{9+x}$ ($x = 0$) Heusler alloy, ZFC and FCC, M vs T curves, measured in different fields under ambient pressure. $M_s$ and $M_f$ indicate the martensitic start and finish temperatures respectively.

martensitic finish temperature ($M_f$) (i.e., around 284 K, which is obtained from the point of inflection in the first derivative of $M$ vs $T$ curves). This is in good agreement with the structural assessment made from XRD data. However, the Curie temperature of the austenite phase ($T_C^A$) for this alloy is not observed until 350 K (our measuring T range). For better clarity, a zoomed-in view of the M vs T curves near the inflection point for different pressures is shown in the inset of Fig. 1(a). With further lowering the temperature below 125 K, a large splitting between ZFC and FCC curves is observed, which may be attributed to the presence of coexisting AFM/FM phases, or spin glass/FM or ferrimagnetic (FI) phases at low temperatures in the martensite phase. Similar bifurcation is reported in many other systems [7,12,18]. With the application of pressure, the characteristic transition temperatures, i.e., $M_s$, $M_f$, austenite start temperature ($A_s$), austenite finish temperature ($A_f$), and $T_C^A$ are found to significantly shift to higher values, which indicates the robust stabilization of the martensite phase with pressure. For $x = 0$ alloy, the magnetization value at $M_s$ decreases with pressure, whereas it almost remains unchanged at $M_f$, which leads to the decrease in magnetization difference ($\Delta M$) between the martensite and austenite phases across the martensitic transition.

For $x = 2$ alloy [Fig. 1(b)], $T_C^A$, $M_s$, and $M_f$ decrease to around 289 K, 110 K, and 49 K respectively, under ambient pressure condition, which are much lower than those for $x = 0$ alloy. This decrease in the martensitic transition temperatures with the increase of x (i.e., Sn content) can be attributed to the decrease in the valence electron concentration (e/a ratio) [19]. For $x = 2$, with the application of pressure, the martensitic transition temperature also increases significantly with pressure, whereas $T_C^A$ decreases marginally with pressure. This suggests that external pressure does not affect the magnetic behavior of its ferromagnetic austenite phase much. However, the martensitic transition is found to be broader for $x = 2$ as compared to that for $x = 0$ alloy and hence the exact estimation of $M_s$ and $M_f$ from inflection point is difficult.

The pressure dependence of $M_s$, $M_f$, $A_s$, $A_f$, and $T_M = (M_s+M_f)/2$ for $x = 0$ alloy is shown in Fig. 2. The pressure derivatives of $M_s$ ($dM_s/dP$) and $T_M$ ($dT_M/dP$) for this alloy are found to be around 3.84 K/kbar and 3.75 K/kbar respectively, which are higher than the reported values in other Heusler alloys, such as in $Ni_2MnGa$ ($dT_M/dP = 0.05$ K/kbar), $Ni_{50}Mn_{36}Sn_{14}$ (2.4 K/kbar), Ni-Mn-In (2 K/kbar), and Ni-Mn-Sn (3.16 and 0.51 K/kbar) [20–23]. The pressure dependence of $M_s$ in both the alloys confirms more robust stabilization of martensite phase with the application of pressure. The change in $M_s$ with pressure is attributed to the change in the volume. As reported in literature, generally the volume of the martensite phase is lower than that of the austenite phase [8]. The application of pressure generally causes a reduction in volume as well as the bond lengths, which then requires more thermal energy to drive the martensitic transition, consequently leading to an increase in the martensitic transition temperatures. This behavior can be explained by the Clausius-Clapeyron equation [8,16],

$$dT/dP = (V_A - V_M)/(S_A - S_M) = \Delta V/\Delta S \qquad (1)$$

where $dT/dP$, $\Delta V$, and $\Delta S$ are the rate of change of transition temperature with respect to pressure, volume, and entropy change across the transition, respectively. It is generally reported that in Mn-Ni-Sn type Heusler alloys, $\Delta S$ and $\Delta V$ are positive [12,16,24], giving rise to $dT/dP \geqslant 0$. Generally, pressure is expected to stabilize the lower volume phase, which is the martensite phase in the present case, as a result of the reduction in interatomic distances in the unit cell.

Apart from the effect of pressure, we have also studied the effect of magnetic field on the martensitic transition. Figure 3 shows the ZFC and FCC M vs T curves recorded at different fields, under ambient pressure for the typical case of $x = 0$ alloy. With increasing field, the martensitic transition slightly shifts to lower temperatures, e.g., 293 K for 1 kOe decreasing to 290 K for 70 kOe. This observation suggests that the application of field leads to the stabilization of the austenite phase in the present alloy, which is opposite to the effect of pressure. This trend matches well with other reports on Heusler systems [8,10,11]. It is clear from the figure that with the application of field, the magnetization of the austenite phase increases significantly as compared to that of the martensite phase, which

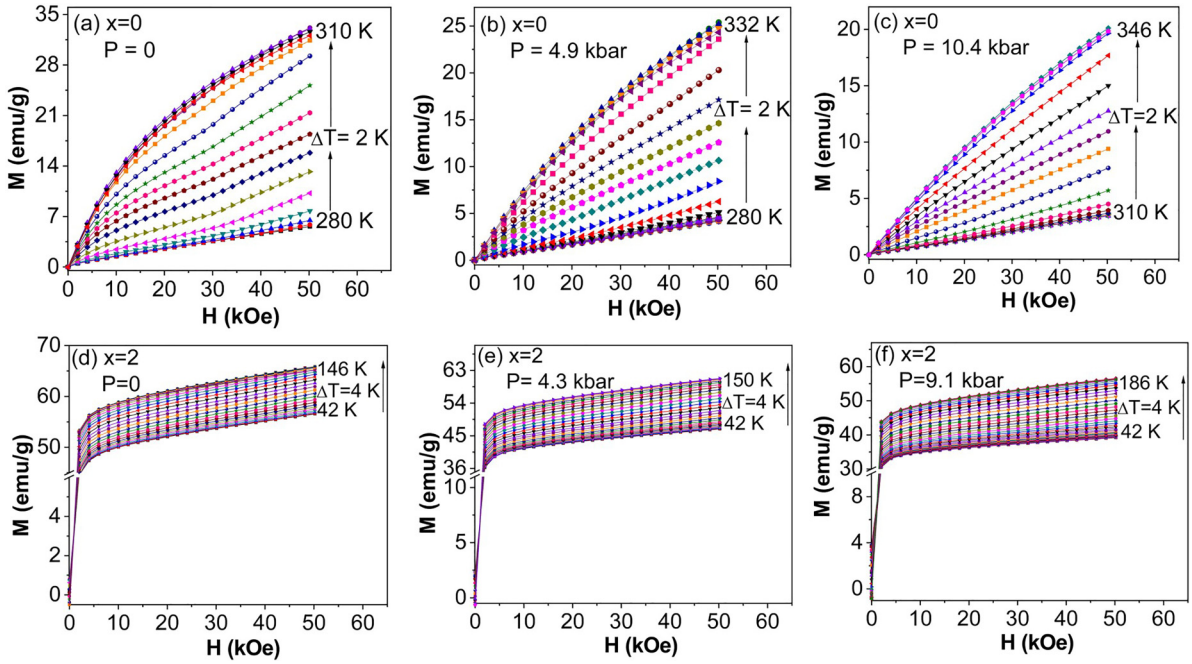


FIG. 4. For $Mn_{50}Ni_{41-x}Sn_{9+x}$ Heusler alloy, magnetization isotherms (M-H curves) measured at different temperatures in the vicinity of the martensitic transition under different applied pressures for (a)–(c) $x = 0$ and (d)–(f) $x = 2$ alloys.

would lead to the increase in ΔM value across the transition, and consequently may give rise to large MCE in this alloy. At low temperatures, the splitting between ZFC and FCC curves is found to decrease with field, indicating the possibility of enhanced FM coupling with field.

To further investigate the effect of pressure on magnetic properties and MCE, the magnetization isotherms (M-H curves) are recorded at different temperatures in the vicinity of martensitic transition, under different applied pressures for both the alloys. The temperature interval (ΔT) of 2 K and 4 K are used for $x = 0$ and 2 respectively, according to the width of the transition in these alloys, as shown in Figs. 4(a)–4(f). Clearly, for $x = 0$ alloy, the magnetization does not saturate even at 50 kOe, which suggests the coexistence of AFM/FM exchange interactions in the alloy. Below 288 K, the M-H curves show a linear behavior, which may be due to the paramagnetic state of the martensite phase. With increasing pressure, the magnetization value is found to decrease across the transition, which may be attributed to the weakening of the FM coupling under pressure, agreeing with the M-T results shown in Fig. 1(a). However, for $x = 2$ alloy [Figs. 4(d)–4(f)], magnetization shows a different behavior, as it gets nearly saturated at 50 kOe, which is attributed to the increase in the FM coupling with the increase in $x$. With the application of pressure, the magnetization value decreases, as in the case of $x = 0$. For $x = 0$, maximum magnetization is around 33.4 emu/g (at 50 kOe) across the transition for P = 0, which decreases to 20 emu/g for P = 10.4 kbar. However, for $x = 2$, the corresponding M values are 66 emu/g (P = 0) and decreases to 56 emu/g (for 9.1 kbar).

It is generally proposed that in Mn rich Mn-Ni-Sn Heusler alloys, the extra Mn atoms occupy the Sn sites as well as the Ni sites, and they couple antiferromagnetically with the regular Mn atoms [12,13,25]. At the same time, the martensitic transition is also seen to shrink the crystallographic axes as a result of the twining of martensite phase variants, which consequently reduce the interatomic distances between different atoms, enhancing the AFM strength in these alloys. Most of the interatomic distances between Mn atoms at different sites in these alloys are expected to be less than the typical bond length of 3 Å in Mn-Ni-Sn alloys, which leads to the AFM coupling between them. The interatomic distances increase with $x$, which explains the strengthening of FM coupling with increasing x. On the contrary, with the application of pressure, as the bond lengths decrease, this would lead to further enhancement of AFM coupling.

Figures 5(a) and 5(b) show the isothermal magnetic entropy change ($\Delta S_M$) as a function of temperature, under different applied pressures for both the alloys. The $\Delta S_M$ has been calculated from the M-H curves measured at different temperatures across the martensitic transition [shown in Figs. 4(a)–4(f)] using the Maxwell's relation [3]. The observed positive values of $\Delta S_M$ for both the alloys confirm

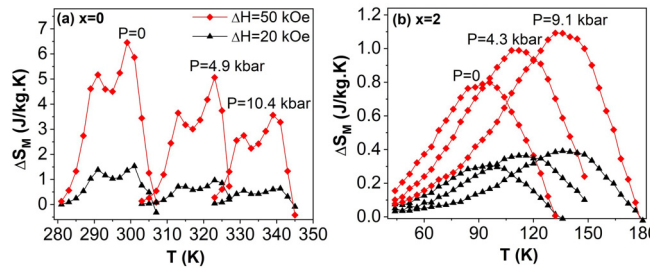


FIG. 5. For $Mn_{50}Ni_{41-x}Sn_{9+x}$ Heusler alloys, isothermal magnetic entropy change ($\Delta S_M$) under different applied pressures for composition (a) $x = 0$ and (b) $x = 2$.

the presence of inverse MCE. For $x = 0$, a maximum $\Delta S_M$ of around 6.5 J/Kg K (at $\Delta H = 50$ kOe) has been obtained at RT under ambient pressure, which is reasonably good for the magnetic refrigeration. This value is found to be larger than that observed in some other Heusler alloys at RT, such as 3 J/Kg K for $Mn_{1.25}Fe_{1.75}Ga$ [26] and 2.1 J/Kg K for $Ni_{41}Co_9Mn_{32}Al_{18}$ alloys [27]. The present value of $\Delta S_M$ at ambient pressure may be attributed to a comparatively sharp magnetostructural transition at ambient pressure for this alloy, which results in large $\Delta M$. However with the application of pressure, the $\Delta S_M$ value decreases, but the peak temperature shifts significantly towards higher values, such as $\Delta S_M =$ 3.6 J/Kg K at 339 K for P = 10.4 kbar (at $\Delta H = 50$ kOe). This decrease in $\Delta S_M$ is due to the decrease in $\Delta M$ (between austenite and martensite phases) across the transition with increasing pressure. In Fig. 5(a), one can notice an extra peak in $\Delta S_M$ curves at lower temperatures for all the applied pressures, which is probably due to an intermediate phase transformation, widely believed to originate mainly from the magnetoelastic coupling between the structural and magnetic degrees of freedom in these Ni-Mn-$X$ ($X$ = Ga, Sn, In) Heusler alloys. Similar nature of two successive positive peaks in $\Delta S_M$ curves has been observed in other Heusler systems as well, which lead to the broadened working temperature interval, owing to the intermediate phase transformation [28,29]. This is also corroborated with the higher fields M vs T curves (Fig. 3), where a shoulder has been observed prior to the martensitic transition for higher measuring field values. But interestingly, for $x = 2$ alloy [see Fig. 5(b)] $\Delta S_M$ shows the opposite trend as compared to $x = 0$, as it increases slightly with the increase in pressure. A maximum $\Delta S_M$ of around 0.8 J/Kg K at 94 K ($\Delta H = 50$ kOe) is found under ambient pressure, which slightly increases to 1.2 J/Kg K at 135 K for P = 9.1 kbar. Clearly $\Delta S_M$ shows broader peaks across the transition for $x = 2$ alloy [Fig. 5(b)] as compared to that for $x = 0$ alloy, which is in good agreement with the M vs T curves [Fig. 1(b)]. The complete negative or positive pressure coefficients of $\Delta S_M$ have been observed separately in many other Heusler systems [9,11,30,31], but the trend observed in the present alloys (i.e., the observation of both negative as well as positive pressure coefficients of $\Delta S_M$ across the martensitic transition in similar alloy series) is rare [11].

Refrigeration capacity (RC) is one of the most essential factors to evaluate the magnetocaloric performance of a material. RC is defined as the amount of heat transferred between cold and hot sinks over a complete refrigeration cycle. We have calculated the RC value using $\Delta S_M$ vs $T$ curves [Figs. 5(a) and 5(b)] for different applied pressures, employing the following equation [32]:

$$\mathrm{RC} = \int_{T1}^{T2} |\Delta S_M(T, \Delta H)| dT \tag{2}$$

where $T_1$ and $T_2$ denote the lower and higher temperatures at half maximum of $\Delta S_M$ peak in $\Delta S_M$ vs $T$ curve, respectively. For $x = 0$, a maximum RC of around 79 J/kg has been observed for P = 0, and decreases to 38 J/kg for P = 10.4 kbar. However, for $x = 2$ alloy, RC is found to increase with the increase in pressure, i.e., from 35 J/kg for P = 0 to 55 J/kg for P = 9.1 kbar. It is interesting to note that $x = 0$ alloy shows a large operating temperature range of 16 K for RC around RT. The decrease/increase in RC value with pressure for $x = 0/2$ alloy is attributed to the change in the width of the martensitic transition region and decrease/increase of $\Delta S_M$ values with pressure. This suggests that the martensitic transition, MCE as well as the RC can be easily tuned at/around RT with the application of external pressure and magnetic field, which makes these alloys interesting from fundamental as well as application perspectives.

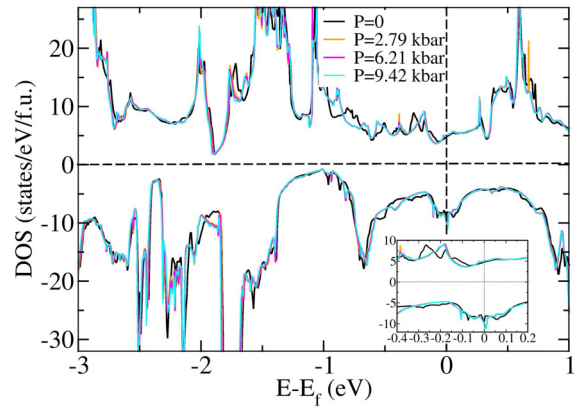


FIG. 6. For stoichiometric $Mn_2NiSn$, spin polarized total density of states (DOS) at different pressures (in FiM state). Inset shows a zoomed-in view near Fermi level ($E_f$).

### B. *Ab Initio* Calculations

To better understand our experimental findings/trends, we have studied the pressure effect on electronic and magnetic properties of the present alloys using *ab initio* density functional theory calculations. First, we have calculated the pressure effect on the ground-state properties of the stoichiometric $Mn_2NiSn$ alloy. At ambient pressure, it is found to show a ferrimagnetic (FiM) ground state, where Mn atoms mainly contribute to the total magnetic moment (i.e., 2.76 μB/f.u.). Table I shows the theoretically optimized lattice parameters, total and atom-projected moments, and the relative energies ($\Delta E_{\mathrm{tot}}$) for nonmagnetic (NM), ferromagnetic (FM), and ferrimagnetic (FiM) phases of $Mn_2NiSn$. Here, two different Mn sublattice (denoted as $Mn_I$ and $Mn_{II}$) moments are found to be oppositely aligned, which partially compensate each other, leading to a finite net magnetization ($\mu_{\mathrm{tot}}$). With the application of pressure (i.e., compressive strain of up to 0.3% (9.42 kbar), the total magnetic moment very slightly changes. Figure 6 shows the pressure dependent spin-resolved density of states (DOS) for the stoichiometric $Mn_2NiSn$ alloy (in the FiM state). A sizable DOS has been observed at the Fermi level for all the pressure values, which confirms the metallic character of this alloy. FiM state can also be clearly seen from the exchange splitting between the two spin channels. Inset of Fig. 6 shows a zoomed-in view of the DOS near $E_f$ for better clarity of the variation in majority and minority spin DOS with pressure. One can clearly see from the figure that with the application of pressure, DOS is found to slightly increase in both the spin channels. The peak observed in minority spin channel around $E_f$ shifts slightly upward with

TABLE I. Theoretically optimized lattice parameters (a = b, c), total magnetic moment ($\mu_{tot}$), atomic projected average moments ($\mu_i$), and the relative energy ($\Delta E_{tot}$) of nonmagnetic (NM), ferromagnetic (FM), and ferrimagnetic (FiM) configurations for stoichiometric $Mn_2NiSn$, off-stoichiometric $Mn_{50}Ni_{41.41}Sn_{8.59}$ (near $x = 0$ composition) and $Mn_{50}Ni_{39.06}Sn_{10.94}$ (near $x = 2$ composition) alloys, at ambient pressure. Here the energy of FiM configuration is taken as the reference.

| Mag. Config. | a = b (Å) | c (Å) | $\mu_{tot}$ ($\mu_B$/f.u.) | $\mu_{MnI}$ ($\mu_B$) | $\mu_{MnII}$ ($\mu_B$) | $\mu_{Ni}$ ($\mu_B$) | $\mu_{Sn}$ ($\mu_B$) | $\Delta E_{tot}$ (eV/f.u.) |
|---|---|---|---|---|---|---|---|---|
| | | | Stoichiometric $Mn_2NiSn$ | | | | | |
| NM | 5.93 | | | | | | | 4.61 |
| FM | 6.03 | | 15.60 | 3.06 | 0.45 | 0.44 | –0.05 | 1.38 |
| FiM | 6.13 | | 2.76 | 3.76 | –2.95 | –0.11 | –0.01 | 0 |
| | | | $x = 0$ | | | | | |
| NM | 10.27 | 13.92 | | | | | | 28.16 |
| FM | 10.40 | 15.06 | 27.29 | 3.05 | 2.88 | 0.50 | –0.18 | 22.57 |
| FiM | 10.40 | 14.86 | 1.10 | 2.95 | –3.10 | 0.19 | –0.05 | 0 |
| | | | $x = 2$ | | | | | |
| NM | 10.33 | 14.01 | | | | | | 28.77 |
| FM | 10.47 | 15.11 | 27.54 | 3.04 | 3.33 | 0.50 | –0.19 | 22.42 |
| FiM | 10.66 | 14.96 | 1.64 | 2.84 | –3.13 | 0.16 | 0.05 | 0 |

pressure, whereas that of majority spin channel remains nearly unchanged.

We further simulated the electronic structure of the representative compositions ($Mn_{50}Ni_{41.41}Sn_{8.59}$ and $Mn_{50}Ni_{39.06}Sn_{10.94}$) using a 2×2×2 supercells, which are closest to the corresponding compositions of the experimentally synthesized samples for $x = 0$ and 2 respectively. For both these compositions, the crystal structure is fully relaxed in different magnetic configurations (i.e., NM, FM, and FiM) under ambient pressure. The theoretically optimized lattice parameters, total and atom projected magnetic moments, and relative energies for different magnetic configurations for $x = 0$ and 2 alloys are listed in Table I. Clearly, for both the alloys, FiM is the ground-state magnetic ordering, with a tetragonal structure (martensitic phase structure) with distortion of $c/a = 1.43$ for $x = 0$, which decreases to 1.40 for $x = 2$ alloy. The Mn-atoms are the major contributor to the total magnetic moment in both the cases. If one compares the magnetic moment of these alloys with the stoichiometric one, the magnetic moment decreases in the former, which indicates the decrease of FM coupling in the off stoichiometric alloys, as compared to the stoichiometric one, as also visible in our experimental results.

Figure 7 shows the spin-resolved DOS for both the alloys at ambient pressure. A finite DOS at $E_F$ in both the cases confirms the metallic character. The FiM ground state is clearly evident from the exchange splitting between the two spin channels, as also observed for the stoichiometric alloy (shown in Fig. 6). However, there are certain visible differences in the DOS profiles for the two alloys, such as the peaks observed in both the spin channels for $x = 2$ alloy shift downward with respect to $E_f$, as compared to that for $x = 0$, which is attributed to the change in valence electron concentration with composition x (i.e., Sn content). A close inspection of the orbital contribution in DOS shows that $d$ orbitals of Mn and Ni atoms are the major contributor at/around $E_f$.

Next, we perform the pressure dependent DFT calculations for these off-stoichiometric alloys. We first apply the external pressure hydrostatically (i.e., compressive strain along all the three directions uniformly up to 0.3% in the energetically lowest FiM state for both the alloys (data not shown here). The total magnetic moment ($\mu_{tot}$) does not change much for both the cases at ambient pressure (see Table I). Application of pressure also has little effect on the total moment, e.g., for $Mn_{50}Ni_{41.41}Sn_{8.59}$, $\mu_{tot}$ is 1.108 μB for P = 0, which changes to 1.110 μB for 10.84 kbar (0.3% compressive strain). This may be due the magnetocrystalline anisotropy, as a result of the tetragonal distortion present in the alloy. This is indeed reported earlier that Heusler alloys show a reasonably large magnetocrystalline anisotropy, mediated by the tetragonal distortion [33,34]. However, in a real material, there is a possibility to exhibit nonuniform strain. To check this effect, we apply uniaxial strain along a certain direction. For $Mn_{50}Ni_{41.41}Sn_{8.59}$ alloy, when the pressure (i.e., compressive strain up to 0.3% is applied along the $c$ axis, the magnetic moment again showed little changes, e.g., at P = 0, it is 1.108 μB, which becomes 1.103 μB at P = 10.17 kbar (0.3% strain). However, when the same pressure is applied along the $a/b$ direction, the total magnetic moment increases appreciably, and the corresponding data is shown in Table II. One can clearly see from the table that the total magnetic moment

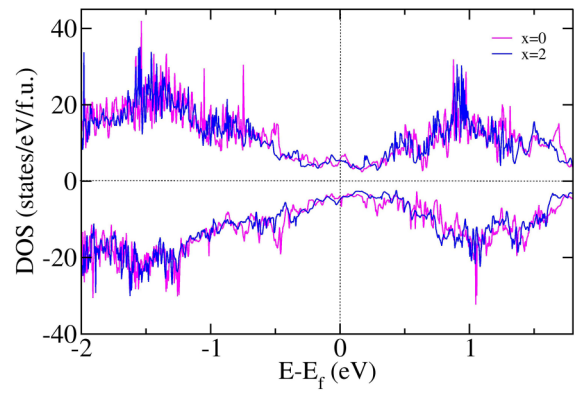


FIG. 7. Spin-resolved density of states of the two off-stoichiometric alloys, $Mn_{50}Ni_{41.41}Sn_{8.59}$ (close to $x = 0$ composition) and $Mn_{50}Ni_{39.06}Sn_{10.94}$ (close to $x = 2$ composition) at ambient pressure in FiM configuration.

TABLE II. For $Mn_{50}Ni_{41.41}Sn_{8.59}$ alloy, variation of total and Mn-projected average magnetic moments, and volume as a function of pressure along $a$ or $b$ axes.

| P (kbar) | Change in $a$ or $b$ (%) | Volume (Å$^3$) | $\mu_{tot}$ ($\mu_B$/f.u.) | $\mu_{MnI}$ ($\mu_B$) | $\mu_{MnII}$ ($\mu_B$) |
|---|---|---|---|---|---|
| 0 | 0 | 1609.77 | 1.108 | 3.033 | –3.069 |
| 3.0 | –0.1 | 1604.89 | 1.148 | 3.023 | –3.061 |
| 7.0 | –0.2 | 1600.07 | 1.156 | 3.012 | –3.052 |
| 11.3 | –0.3 | 1595.28 | 1.162 | 3.002 | –3.045 |

TABLE III. For $Mn_{50}Ni_{39.06}Sn_{10.94}$ alloy, variation of total and Mn-projected average magnetic moments, and volume as a function of pressure along $c$ axes.

| P (kbar) | Change in $c$ (%) | Volume (Å$^3$) | $\mu_{tot}$ ($\mu_B$/f.u.) | $\mu_{MnI}$ ($\mu_B$) | $\mu_{MnII}$ ($\mu_B$) |
|---|---|---|---|---|---|
| 0 | 0 | 1638.79 | 1.643 | 3.146 | –3.122 |
| 5 | –0.1 | 1633.16 | 1.618 | 3.135 | –3.112 |
| 8.5 | –0.2 | 1628.47 | 1.597 | 3.127 | –3.099 |
| 12.2 | –0.3 | 1624.06 | 1.577 | 3.119 | –3.064 |

TABLE IV. For $Mn_{50}Ni_{41.41}Sn_{8.59}$ alloy, simulated bond lengths between different neighboring pairs at ambient pressure and P = 11.3 kbar.

| | Bond length (at P = 0) (Å) | Bond length (at P = 11.3 kbar) (Å) |
|---|---|---|
| $Mn_{II}$-Ni | 2.48 | 2.59 |
| $Mn_I$-Ni | 2.46 | 2.59 |
| $Mn_{II}$-Sn | 2.59 | 2.77 |
| $Mn_I$-Sn | 2.60 | 2.59 |
| $Mn_{II}$-$Mn_I$ | 2.46 | 2.47 |

increases from 1.108 μB at P = 0 to 1.162 μB at 11.33 kbar. This calculated trend in magnetic moments with pressure is in good agreement with our experimental results [see Fig. 1(a)].

Along the same lines, we have done the pressure dependent calculations for $Mn_{50}Ni_{39.06}Sn_{10.94}$ alloy. In case of hydrostatic (uniform compression along all three directions) and pressure along $a/b$ directions, the magnetic moment changes negligibly, such as for a typical case of pressure applied along all the directions, the magnetic moment changes from 1.643 μB at P = 0 to 1.645 μB at 12.78 kbar (0.3% strain). But when the same external pressure is applied along the $c$ axis, the total magnetic moment decreases appreciably. The simulated data at few representative pressures are listed in Table III. This trend agrees fairly well with our experimental results [shown in Fig. 1(b)]. Comparing the total magnetic moment of both the alloys, it is clear that the net moment increases with increase in x. It is important to note that, although the experimentally applied pressure values are slightly different than the theoretically applied pressure values, the overall trend of net moment with increasing pressure matches well. Interestingly, it is the compressive strain along $a/b$ direction, which explains the experimental magnetization trend in one case ($x = 0$), while the same pressure needs to be along $c$ axis to explain the trend observed in the other case ($x = 2$). This may be attributed to the different magnetocrystalline anisotropy present in these alloys.

Figures 8(a) and 8(b) show a comparison of the spin-resolved DOS at different external pressure for the two off-stoichiometric alloys in FiM configuration. A finite DOS at $E_f$ for all pressure values confirms their metallic character. For $x = 0$ alloy, pressure is applied along $a/b$ direction, whereas for $x = 2$ alloy, it is applied along $c$ axis, as discussed above. Clearly, the DOS profiles does not change much with varying pressure specially at/near $E_F$. However, it indeed affects the magnetic properties appreciably, even when applied pressure is not too large [9,35].

To better understand the trend in the magnetic properties and the exchange mechanism under applied pressure, we have calculated the bond lengths between nearest-neighbor Mn and other constituent elements at ambient condition and the maximum pressure applied for both the alloys, as listed in Tables IV and V respectively. As discussed earlier, in Mn rich Mn-Ni-Sn Heusler alloys, the exchange interactions between the Mn moments get strongly influenced by the distance between them at different sites. It is generally observed that, in Mn-rich Mn-Ni-Sn alloys, the coupling between regular Mn atoms and Mn atoms at the Ni and Sn sites are predominantly

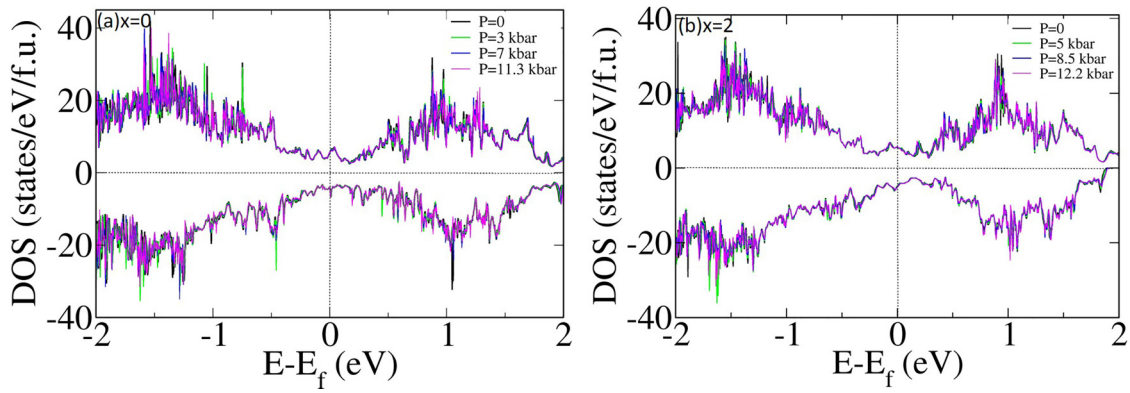


FIG. 8. Comparison of spin-resolved density of states at various pressures for $Mn_{50}Ni_{41.41}Sn_{8.59}$ (left) and $Mn_{50}Ni_{39.06}Sn_{10.94}$ (right) alloys in FiM configuration. Fermi level ($E_f$) is set at 0 eV.

TABLE V. For $Mn_{50}Ni_{39.06}Sn_{10.94}$ alloy, simulated bond lengths between different neighboring pairs at ambient pressure and P = 12.2 kbar.

| | Bond length (at P = 0) (Å) | Bond length (at P = 12.2 kbar) (Å) |
|---|---|---|
| $Mn_{II}$-Ni | 2.49 | 2.47 |
| $Mn_{I}$-Ni | 2.62 | 2.48 |
| $Mn_{II}$-Sn | 2.76 | 2.73 |
| $Mn_{I}$-Sn | 2.60 | 2.55 |
| $Mn_{II}$-$Mn_{I}$ | 2.49 | 2.45 |

of AFM type due to decrease in interatomic distances less than a critical value [36]. From Tables IV and V, one can clearly see that the interatomic distances between inequivalent Mn atoms and the neighboring atoms are less than the critical value, which suggests AFM coupling between them. However, the interatomic distances between the equivalent Mn atoms (e.g., $Mn_I$-$Mn_I$) are greater than this value, which indicates FM coupling. These bond lengths also suggest that there is a possibility of coexistence of AFM/FM exchange interactions at low temperatures in these alloys, which is in good agreement with our experimental results [i.e., the spitting between ZFC and FCC M vs T curves, as shown in Figs. 1(a) and 1(b)]. Apart from that, it is evident from the Tables that at ambient pressure, the interatomic distances are larger for $x = 2$ as compared to $x = 0$, which is responsible for the enhancement of FM coupling with increasing x. However, with the application of pressure, these interatomic distances between different atoms show opposite trend in the two alloys (see Tables IV and V). This suggests that application of pressure leads to the suppression (enhancement) of AFM coupling in $x = 0$ ($x = 2$) alloys, such as for $x = 0$ alloy, when compressive strain of 0.3% (i.e., P = 11.3 kbar) is applied, the interatomic distances have been found to increase as compared to that with P = 0 pressure. While on the other hand for $x = 2$ alloy, when the compressive strain of 0.3% (i.e. P = 12.2 kbar) is applied, the interatomic distances have been found to decrease as compared to that with P = 0. These trends on interatomic distances with pressure are in fair agreement with the experimental results shown in Figs. 1(a) and 1(b) for these alloys, where the magnetization of FCC M vs T curves has been found to increase with pressure for $x = 0$ alloy, while it decreases with pressure for $x = 2$ alloy.

## IV. CONCLUSIONS

In summary, we report the effect of pressure and magnetic field on the martensitic transition, magnetic, and magnetocaloric properties in off-stoichiometric $Mn_{50}Ni_{41-x}Sn_{9+x}$ ($x = 0$ and 2) Heusler alloys using a combined experimental and theoretical study. At room temperature (RT), $x = 0$ alloy possesses the mixed structure (involving tetragonal and cubic phase), whereas $x = 2$ alloy crystallizes in a cubic structure. Martensitic transition temperature ($T_M$) increases with increasing pressure in both the alloys, confirming robust stabilization of the martensite phase with pressure. In contrast, application of external magnetic field helps to stabilize the austenite phase, as $T_M$ decreases marginally with field. A maximum magnetic entropy change ($\Delta S_M$) of 6.5 J/Kg K is observed at RT under ambient pressure for $x = 0$ alloy, which is comparable to many other Heusler systems, indicating its usefulness for magnetic refrigeration applications. Interestingly, $\Delta S_M$ decreases with increasing pressure for $x = 0$, but shows an opposite trend for $x = 2$ alloy. This is attributed to the change in magnetization difference between the two phases across the martensitic transition. Similar to $\Delta S_M$, refrigeration capacity (RC) is also found to decrease/increase with pressure for $x = 0/2$ alloys. While the magnetization at low temperatures has a reverse trend under pressure for the two alloys. *Ab initio* calculations confirm a ferrimagnetic (FiM) ordering with a finite net magnetization and tetragonal distortion, agreeing well with our experimental findings. The measured trend of magnetization is attributed to the nonuniform effect of in-plane and out-of-plane strain on the magnetic properties, which in turn may arise due to the large magnetocrystalline anisotropy present in these alloys. This can also be correlated with the effect of varying bond lengths between different magnetic species in the alloys and hence the antiferromagnetic/ferromagnetic exchange coupling strengths under pressure. The present study suggests that by combining suitable parameters such as external pressure, composition, and magnetic field, one can tune the martensitic transition, magnetic and magnetocaloric properties of such useful Heusler alloys.

## ACKNOWLEDGMENT

J.S. thanks Department of Science and technology (DST)for the financial support via the DST Women Scientist program (Grant No. DST/WOS-A/PM-77/2019).

[1] V. K. Pecharsky and K. A. Gschneidner, Jr., Giant magnetocaloric effect in $Gd_5(Si_2Ge_2)$, Phys. Rev. Lett. **78**, 4494 (1997).

[2] A. Planes, L. Manosa, and M. Acet, Magnetocaloric effect and its relation to shape-memory properties in ferromagnetic Heusler alloys, J. Phys.: Condens. Matter **21**, 233201 (2009).

[3] A. M. Tishin and Y. I. Spichkin, *The Magnetocaloric Effect and Its Application* (IOP Publishing, Bristol, UK, 2003).

[4] M. Pasquale, C. P. Sasso, L. H. Lewis, L. Giudici, T. Lograsso, and D. Schlagel, Magnetostructural transition and magnetocaloric effect in $Ni_{55}Mn_{20}Ga_{25}$ single crystals, Phys. Rev. B **72**, 094435 (2005).

[5] A. Sozinov, A. A. Likhachev, N. Lanska, and K. Ullakko, Giant magnetic-field-induced strain in NiMnGa seven-layered martensitic phase, Appl. Phys. Lett. **80**, 1746 (2002).

[6] A. K. Pathak, I. Dubenko, C. Pueblo, S. Stadler, and N. Ali, Magnetoresistance and magnetocaloric effect at a structural phase transition from a paramagnetic martensitic state to a paramagnetic austenitic state in $Ni_{50}Mn_{36.5}In_{13.5}$ Heusler alloys, Appl. Phys. Lett. **96**, 172503 (2010).

[7] A. K. Nayak, K. G. Suresh, and A. K. Nigam, Observation of enhanced exchange bias behaviour in NiCoMnSb Heusler alloys, J. Phys. D: Appl. Phys. **42**, 115004 (2009).

[8] L. Mañosa, X. Moya, A. Planes, O. Gutfleisch, J. Lyubina, M. Barrio, J. L. Tamarit, S. Aksoy, T. Krenke, and M. Acet, Effects of hydrostatic pressure on the magnetism and martensitic transition of Ni-Mn-In magnetic superelastic alloys, Appl. Phys. Lett. **92**, 012515 (2008).

[9] F. Albertini, J. Kamarad, Z. Arnold, L. Pareti, E. Villa, and L. Righi, Pressure effects on the magnetocaloric properties of Ni-rich and Mn-rich $Ni_2MnGa$ alloys, J. Magn. Magn. Mater. **316**, 364 (2007).

[10] A. K. Nayak, K. G. Suresh, A. K. Nigam, A. A. Coelho, and S. Gama, Pressure induced magnetic and magnetocaloric properties in NiCoMnSb Heusler alloy, J. Appl. Phys. **106**, 053901 (2009).

[11] S. E. Muthu, M. Kanagaraj, S. Singh, P. U. Sastry, G. Ravikumar, N. V. Rama Rao, M. Manivel Raja, and S. Arumugam, Hydrostatic pressure effects on martensitic transition, magnetic and magnetocaloric effect in Si doped Ni-Mn-Sn Heusler alloys, J. Alloys Compd. **584**, 175 (2014).

[12] G. D. Liu, J. L. Chen, Z. H. Liu, X. F. Dai, G. H. Wu, B. Zhang, and X. X. Zhang, Martensitic transformation and shape memory effect in a ferromagnetic shape memory alloy: $Mn_2NiGa$, Appl. Phys. Lett. **87**, 262504 (2005).

[13] J. Sharma and K. G. Suresh, Investigation of multifunctional properties of $Mn_{50}Ni_{40-x}Co_xSn_{10}$ ($x = 0$–6) Heusler alloys, J. Alloys Compd. **620**, 329 (2015).

[14] J. Ren, H. Li, S. Feng, Q. Zhai, J. Fu, Z. Luo, and H. Zheng, Giant magnetocaloric effect in a Heusler $Mn_{50}Ni_{40}In_{10}$ unidirectional crystal, Intermetallics **65**, 10 (2015).

[15] J. Sharma and K. G. Suresh, Observation of giant exchange bias in bulk $Mn_{50}Ni_{42}Sn_8$ Heusler alloy, Appl. Phys. Lett. **106**, 072405 (2015).

[16] L. Ma, W. H. Wang, J. B. Lu, J. Q. Li, C. M. Zhen, D. L. Hou, and G. H. Wu, Coexistence of reentrant-spin-glass and ferromagnetic martensitic phases in the $Mn_2Ni_{1.6}Sn_{0.4}$ Heusler alloy, Appl. Phys. Lett. **99**, 182507 (2011).

[17] See Supplemental Material at http://link.aps.org/supplemental/10.1103/PhysRevB.109.064418 for auxiliary information about XRD at room temperature for present alloys.

[18] D. Y. Cong, S. Roth, and L. Schultz, Magnetic properties and structural transformations in NiCoMnSn multifunctional alloys, Acta Mater. **60**, 5335 (2012).

[19] T. Krenke, X. Moya, S. Aksoy, M. Acet, P. Entel, L. Manosa, A. Planes, Y. Elerman, A. Yucel, and E. F. Wassermann, Electronic aspects of the martensitic transition in NiMn based Heusler alloys, J. Magn. Magn. Mater. **310**, 2788 (2007).

[20] U. Devarajan, S. E. Muthu, S. Arumugam, S. Singh, and S. R. Barman, Investigation of the influence of hydrostatic pressure on the magnetic and magnetocaloric properties of $Ni_{2-x}Mn_{1+x}Ga$ ($x = 0, 0.15$) Heusler alloys, J. Appl. Phys. **114**, 053906 (2013).

[21] S. E. Muthu, N. V. Rama Rao, M. Manivel Raja, S. Arumugam, K. Matsubayasi, and Y. Uwatoko, Hydrostatic pressure effect on the martensitic transition, magnetic, and magnetocaloric properties in $Ni_{50-x}Mn_{37+x}Sn_{13}$ Heusler alloys, J. Appl. Phys. **110**, 083902 (2011).

[22] T. Yasuda, T. Kanomata, T. Saito, H. Yosida, H. Nishihara, R. Kainuma, K. Oikawa, K. Ishida, K. U. Neumann, and K. R. A. Ziebeck, Pressure effect on transformation temperatures of ferromagnetic shape memory alloy $Ni_{50}Mn_{36}Sn_{14}$, J. Magn. Magn. Mater. **310**, 2770 (2007).

[23] M. K. Chattopadhyay, V. K. Sharma, A. Chouhan, P. Arora, and S. B. Roy, Combined effect of hydrostatic pressure and magnetic field on the martensitic transition in the $Ni_{49}CuMn_{34}In_{16}$ alloy, Phys. Rev. B **84**, 064417 (2011).

[24] W. Zhigang, L. Zhuhong, Y. Hong, L. Yinong, and W. Guangheng, Martensitic and magnetic transformation behaviours in $Mn_{50}Ni_{42-x}Sn_8Co_x$ polycrystalline alloys, J. Phys. D: Appl. Phys. **44**, 385403 (2011).

[25] D. Hobbs, J. Hafner, and D. Spisak, Understanding the complex metallic element Mn. I. Crystalline and noncollinear magnetic structure of $\alpha$-Mn, Phys. Rev. B **68**, 014407 (2003).

[26] A. A. El-Gendy and G. C. Hadjipanayis, Room temperature magnetocaloric effect in $Mn_{1.25}Fe_{1.75}Ga$ Heusler alloys, J. Alloys Compd. **665**, 319 (2016).

[27] Y. Kim, E. J. Kim, K. Choi, W. B. Han, H. S. Kim, Y. Shon, and C. S. Yoon, Room-temperature magnetocaloric effect of Ni-Co-Mn-Al Heusler alloys, J. Alloys Compd. **616**, 66 (2014).

[28] X. Zhang, M. Qian, S. Miao, R. Su, Y. Liu, L. Geng, and J. Sun, Enhanced magnetic entropy change and working temperature interval in Ni-Mn-In-Co alloys, J. Alloys Compd. **656**, 154 (2016).

[29] S. C. Ma, H. C. Xuan, C. L. Zhang, L. Y. Wang, Q. Q. Cao, D. H. Wang, and Y. W. Du, Investigation of the intermediate phase and magnetocaloric properties in high-pressure annealing Ni-Mn-Co-Sn alloy, Appl. Phys. Lett. **97**, 052506 (2010).

[30] Y. Sun, J. Kamarad, Z. Arnold, Z. Kou, and Z. Cheng, Tuning of magnetocaloric effect in a $La_{0.69}Ca_{0.31}MnO_3$ single crystal by pressure, Appl. Phys. Lett. **88**, 102505 (2006).

[31] L. Morellon, Z. Arnold, C. Magen, C. Ritter, O. Prokhnenko, Y. Skorokhod, P. A. Algarabel, M. R. Ibarra, and J. Kamarad, Pressure enhancement of the giant magnetocaloric effect in $Tb_5(Si_2Ge_2)$, Phys. Rev. Lett. **93**, 137201 (2004).

[32] K. A. Gschneidner Jr, V. K. Pecharsky, A. O. Pecharsky, and C. B. Zimm, Recent developments in magnetic refrigeration, Mater. Sci. Forum **315-317**, 69 (1999).

[33] A. K. Nayak, M. Nicklas, S. Chadov, P. Khuntia, C. Shekhar, A. Kalache, M. Baenitz, Y. Skourski, V. K. Guduru, A. Puri *et al.*, Design of compensated ferrimagnetic Heusler alloys for giant tunable exchange bias, Nat. Mater. **14**, 679 (2015).

[34] J. Sharma, K. G. Suresh, and A. Alam, Large exchange bias in Mn-Ni-Sn Heusler alloys: Role of cluster spin glass state, Phys. Rev. B **107**, 054405 (2023).

[35] I. Shigeta, Y. Fujimoto, R. Ooka, Y. Nishisako, M. Tsujikawa, R. Y. Umetsu, A. kiko Nomura, K. Yubuta, Y. Miura, T. Kanomata, M. Shirai, J. Gouchi, Y. Uwatoko, and M. Hiroi, Pressure effect on the magnetic properties of the half-metallic Heusler alloy $Co_2TiSn$, Phys. Rev. B **97**, 104414 (2018).

[36] T. Kasuya, Exchange mechanisms in Heusler alloys: Virtual double exchange, Solid State Commun. **15**, 1119 (1974).